Lymph-borne Chemokines and Other Low Molecular Weight Molecules Reach High Endothelial Venules via Specialized Conduits While a Functional Barrier Limits Access to the Lymphocyte Microenvironments in Lymph Node Cortex

By J. Elizabeth Gretz,* Christopher C. Norbury,‡ Arthur O. Anderson,§ Amanda E.I. Proudfoot,‖ and Stephen Shaw*

*From the *Experimental Immunology Branch, National Cancer Institute, and the ‡Laboratory of Viral Diseases, National Institute of Allergy and Infectious Diseases, National Institutes of Health, Bethesda, Maryland 20892; the §Laboratory of Mucosal Immunology, U.S. Army Medical Research Institute for Infectious Diseases, Fort Detrick, Maryland 21712; and the ‖Serono Pharmaceutical Research Institute, 1228 Plan-Les-Ouates/Geneva, Switzerland*

Abstract

Lymph-borne, soluble factors (e.g., chemokines and others) influence lymphocyte recirculation and endothelial phenotype at high endothelial venules (HEVs) in lymph node cortex. Yet the route lymph-borne soluble molecules travel from the subcapsular sinus to the HEVs is unclear. Therefore, we injected subcutaneously into mice and rats a wide variety of fluorophore-labeled, soluble molecules and examined their distribution in the draining lymph nodes. Rather than percolating throughout the draining lymph node, all molecules, including microbial lipopolysaccharide, were very visible in the subcapsular and medullary sinuses but were largely excluded from the cortical lymphocyte microenvironments. Exclusion prevailed even during the acute lymph node enlargement accompanying viral infection. However, low molecular mass (MW) molecules, including chemokines, did gain entry into the cortex, but in a very defined manner. Low MW, fluorophore-labeled molecules highlighted the subcapsular sinus, the reticular fibers, and the abluminal and luminal surfaces of the associated HEVs. These low MW molecules were in the fibers of the reticular network, a meshwork of collagen fibers ensheathed by fibroblastic reticular cells that connects the subcapsular sinus floor and the HEVs by intertwining with their basement membranes. Thus, low MW, lymph-borne molecules, including chemokines, traveled rapidly from the subcapsular sinus to the HEVs using the reticular network as a conduit.

Key words: reticular network • mouse • rat • lymphocyte recirculation • antigen

Introduction

Determining how elements of the immune system come together and interact in lymphoid tissues is important to understanding the immune response and its dysregulation. Much progress has been made in ascertaining the cellular and molecular events of lymphocyte homing and recirculation, and APC–lymphocyte interactions. However, although the anatomy of the lymphoid tissues in which these processes occur is well documented, the roles lymphoid structures play in the orchestration of immune responses remain to be fully understood.

Lymphocytes recirculate through the body via the bloodstream to lymphoid tissue, such as lymph nodes, where they search for their respective antigens, then return to the bloodstream via efferent lymphatics and the thoracic duct (1). Lymphocytes enter the cortex of the lymph node by adhering to and migrating across specialized postcapillary venules called high endothelial venules (HEVs),[1] found in

Portions of this work have appeared in abstract form (1997. *FASEB J.* 11: 687).

Address correspondence to Stephen Shaw, Human Immunology Section, Experimental Immunology Branch, National Cancer Institute, National Institutes of Health, Bldg. 10, Rm. 4B36, 10 Center Dr., MSC 1360, Bethesda, MD 20892. Phone: 301-435-6499; Fax: 301-496-0887; E-mail: sshaw@nih.gov

[1]*Abbreviations used in this paper:* GAG, glycosaminoglycan; HEL, hen egg lysozyme; HEV, high endothelial venule; HRP, horseradish peroxidase; LCA, lens culinaris agglutinin; MIP, macrophage inflammatory protein; MR, hydrodynamic radius; PSA, pisum sativum agglutinin; RANTES, regulated upon activation, normal T cell expressed and secreted; SLC, secondary lymphoid tissue chemoattractant; TEM, transmission electron microscopy; WGA, wheat germ agglutinin.

the T cell–dependent area of the cortex. This process occurs by an adhesion cascade which includes: (a) rolling of the lymphocyte on the luminal surface of an HEV, (b) the presence of a chemokine bound to the endothelial glycocalyx on the HEV luminal surface triggering the activation of the integrins on the surface of the lymphocyte, (c) which allow a firm adherence of the lymphocyte to the endothelium, and finally, (d) migration of the lymphocyte through the wall of the HEV into the lymph node parenchyma (2, 3).

Our studies stemmed from a paradox in chemokine distribution: the presence of macrophage inflammatory protein (MIP)-1β on the luminal surface of HEVs in the cortex of a reactive lymph node (4). The presence of a T cell chemotactic agent on the surface of HEVs is consistent with a role as an inducer of lymphocyte–endothelial interactions. However, MIP-1β is not normally expressed by endothelium (5–7). Interestingly, several studies suggest that the chemokine need not be synthesized locally in the lymph node but rather may be lymph borne. The subcutaneous injection of the chemokine, secondary lymphoid tissue chemoattractant (SLC), into SLC-deficient mice results in a detectable accumulation of SLC and adherent lymphocytes on the luminal surface of HEVs in the draining lymph node (8). Increased lymphocyte emigration from HEVs into the cortex of the draining lymph node occurs within 3 min after a T cell–attracting concentration of IL-8 is injected into the footpad (9). On the other hand, if afferent lymphatics are ligated, the endothelium of HEVs flattens, loses expression of L-selectin addressin, and there is a drastic reduction in the number of lymphocytes emigrating into the lymph node (10–13). Clearly, lymph-borne material from draining tissues, which may include chemokines, not only reaches the HEVs in lymph nodes but may play an important role in maintenance of high endothelial morphology and lymphocyte migration from HEV into lymph node cortex.

Previous studies have suggested that afferent lymph-borne material enters the subcapsular sinus and percolates throughout the lymph node. This would suggest that draining lymph diffuses through the lymph node parenchyma to the HEVs. Nordmann (14) suggested that lymph travels through the lymph node via the subcapsular and medullary sinuses, but a small portion of lymph crosses into the cortical parenchyma where it eventually finds its way into the medullary sinus. Carbon and iron particles and bacterial components are present in the sinuses as well as the cortical parenchyma beneath the subcapsular sinus after intralymphatic administration (14–19). However, it should be noted that other studies demonstrate exclusion of the bulk of carbon particles from the parenchyma of the cortex (20–22). Structural studies of the lymph node sinus walls add additional evidence for the accessibility of the lymph node cortex by lymph. The wall of the subcapsular sinus that is next to the parenchyma is composed of a layer of sinus endothelial cells separated from a layer of fibroblastic reticular cells that face the parenchyma by basement membrane and extracellular matrix (23). The integrity of the floor of the subcapsular sinus is a subject of conflicting reports. Ultrastructural studies demonstrate gaps (0.1–1 μm) or pores in the floor of the subcapsular sinus by electron microscopy (23–26). An additional study argues against the evidence of gaps in the floor of the subcapsular sinus (27). Thus, despite the putative existence of pores in the floor of the subcapsular sinus, there is evidence that penetration of particulate material from lymph into lymph node cortex is attenuated.

Movement of lymph-borne, soluble material into the cortex may be governed by different rules than particulate material. Two intriguing studies demonstrate that although lymph-borne, soluble molecules filling the sinuses cross into the cortex, they do not appear to move freely through the cortical parenchyma of rat lymph nodes. Rather, they preferentially associate with the reticular network, as well as highlighting the HEVs (22, 28). The reticular network is the infrastructure of the lymph node. It is a meshwork of collagen fibers that extend from the capsule throughout the node, suspending blood vessels and sinuses. Interestingly, the reticular network connects the floor of the subcapsular sinus to HEVs by interweaving its collagen fibers with the collagen fibers in both the extracellular matrix of the sinus endothelium and the basement membranes of the HEVs (23, 29). These reticular fibers are ensheathed by fibroblastic reticular cells (23, 30), thus creating an extracellular space that is separate from the space that surrounds the lymphocytes (23). Not only could the reticular network act as a conduit for the movement of soluble, lymph-borne material from the subcapsular sinus to the HEV, but the restriction of soluble material to the "conduit" would also protect the milieu of the lymphocyte microenvironments (22, 23, 28, 31–34).

Given the importance of biological mediators in regulating lymphocyte migration and responses, it is essential to understand the rules of distribution of lymph-borne, soluble molecules, such as chemokines, through the cortex and to the HEVs. Consequently, we have systematically analyzed distribution of a diverse group of fluorophore-labeled, soluble molecules in rat and mouse lymph nodes following subcutaneous injection. In these studies, fluorophore-labeled molecules, draining into the lymph node from the afferent lymphatic vessel, filled the subcapsular and medullary sinuses. The majority of molecules examined were largely excluded from the cortical parenchyma. Instead, low molecular mass (MW) molecules, including chemokines, moved from the subcapsular sinus to the HEVs via the reticular network. Rather than a generalized percolation of soluble lymph-borne molecules throughout the parenchyma of the lymph node, these studies demonstrated a compartmentalization of soluble materials within the T cell–dependent areas of lymph nodes.

Materials and Methods

Soluble Molecules

All soluble molecules used in these experiments were diluted in sterile PBS unless otherwise noted. All subcutaneous injections were 20 μl per site.

Reagents, the concentrations used, and their sources are as follows: acridine orange, hen egg lysozyme (HEL), LPS-FITC (*Escherichia coli*, serotype 055:B5), and horseradish peroxidase (HRP; type VI-A) were from Sigma-Aldrich. HEL-FITC was a gift of Caetano Reis e Sousa (National Institute of Allergy and Infectious Diseases). Acridine orange, HEL-FITC, LPS-FITC, and HRP were used at 5, 7.5, 5, and 10 mg/ml, respectively. OVA-FITC was obtained from Molecular Probes and used at 100 μg/ml. Lysine-fixable, fluorophore-conjugated dextrans were obtained from Molecular Probes and were injected at 5 mg/ml. Both Texas red–labeled, lysine-fixable dextrans (3, 10, 70, and 2,000 kD) and fluorescein-labeled, lysine-fixable, anionic dextrans (3, 10, 40, 70, 500, and 2,000 kD) were used. Lysine-fixable dextrans have covalently bound lysine residues, which covalently bind to the immediately surrounding tissue upon aldehyde fixation. These modified dextrans were used after preliminary studies showed that, despite aldehyde fixation, generic fluorophore-labeled dextrans washed out of tissue sections during slide preparation for microscopy. Anti–mouse MHC class I–FITC (clone AF6-88.5; BD PharMingen) and mouse anti–human CD3-FITC (Becton Dickinson) were injected at 50 and 100 μg/ml, respectively. Cy-Chrome–labeled anti–mouse CD45R/B220 was applied topically to sections on slides at 0.5 μg/ml. FITC-labeled lectins (Vector Laboratories) wheat germ agglutinin (WGA), lens culinaris agglutinin (LCA), or pisum sativum agglutinin (PSA) were injected at 100 μg/ml and applied topically to sections on slides at 20 μg/ml. Fluorophore-labeled regulated upon activation, normal T cell expressed and secreted (RANTES), MIP-1α, and IL-8 (FITC, Cy5) were prepared as described (35). Lyophilized chemokine (10 μg) was dissolved in sterile water (90 μl), then diluted with 10 μl of sterile 10× PBS.

Animals, Animal Preparation, and Injection of Soluble Molecules

All animals were kept in pathogen-free facilities and treated according to National Institutes of Health guidelines.

Dextran and HRP Distribution Studies in Rat Mesenteric Lymph Nodes. Sprague Dawley and Wistar rats (250–400 g; Charles River Laboratories) were anesthetized intramuscularly with sodium pentobarbital (25 mg/kg; Abbott Laboratories) and ketamine HCl (30 mg/kg; Fort Dodge). A midline abdominal incision opened the peritoneal cavity. The caecum and a few loops of the ileum were exteriorized onto a lucite stage using sterile applicators and superfused with bicarbonate-buffered saline. The saline was kept at 37°C and equilibrated with 5% CO_2 in N_2 to a pH of 7.4. Each Peyer's patch was injected with 0.01–0.02 ml of HRP- or fluorophore-labeled dextrans using a 28-gauge needle on a 0.5-ml disposable insulin syringe that has 0.01-ml increments (U-100; Becton Dickinson). Mesenteric lymph nodes were excised between 3 and 30 min and immersion fixed. For transmission electron microscopy (TEM) studies of HRP distribution in lymph nodes, HRP was directly injected intralymphatically and the mesenteric lymph nodes of Wistar rats were prepared for electron microscopy as described by Anderson and Anderson (22).

Dextran, Tracer, Protein, Antibody, and Chemokine Distribution in Peripheral Lymph Nodes. Normal female C57BL/6 mice (National Cancer Institute Animal Production Area) or Sprague Dawley or Wistar rats were anesthetized intraperitoneally with sodium pentobarbital (25 mg/kg; Abbott Laboratories) and ketamine HCl (30 mg/kg; Fort Dodge). Each footpad and lip was injected, subcutaneously, with 0.01–0.02 ml of a soluble molecule solution using the disposable syringes (Becton Dickinson) described above. Draining lymph nodes from the anesthetized animals were harvested between 3 and 10 min or 30 min after injection. These times were chosen after preliminary studies showed that the distribution of soluble molecules was complete in lymph nodes that had been excised and immersion fixed within 2 min of the injection. For 4-h time points, animals were anesthetized for injection and then again for harvest. The superficial cervical, brachial, axillary, inguinal, and popliteal lymph nodes were harvested (a total of 14 lymph nodes per animal). The distribution of each soluble molecule was examined in the lymph nodes of three or more mice, each mouse on a different occasion. In a typical experiment, five mice were used where four mice were injected, each with a different soluble molecule. The lymph nodes from those four mice were compared with that of the fifth mouse, which acted as the control. Note that B10.BR mice (The Jackson Laboratory) were used for the HEL-FITC distribution studies.

Dextran Distribution after Lymph Node Enlargement due to Vaccinia Viral Infection

Vaccinia virus is a member of the poxvirus family that causes a rapid and dramatic increase in draining lymph node size after in-

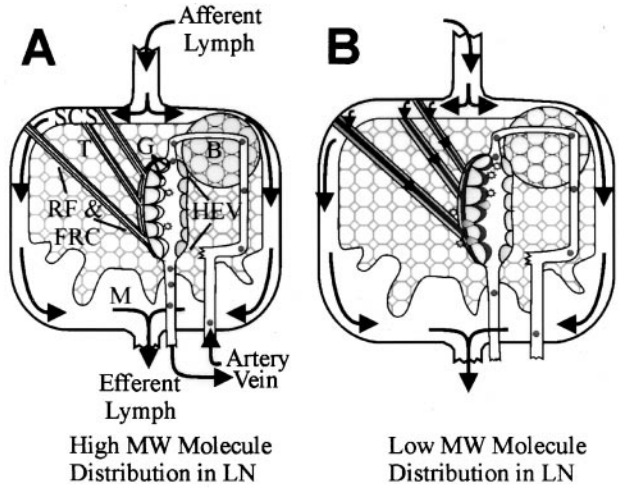

C	SOLUBLE MOLECULES	
FLUID SPACE	HIGH MW	LOW MW
SINUSES	++	++
RETICULAR FIBER CONDUIT	-	++
HEV PERIVENULAR SPACE	-	++
HEV LUMEN/ GLYCOCALYX	-	++
PARENCHYMAL INTERSTITIAL	-	+/-

Figure 1. A model of movement of lymph-borne, soluble molecules through the lymph node; distribution is dependent on molecular size. Rather than percolating through the cortical parenchyma, soluble molecules of both high and low MW moved through the lymph node via the subcapsular and medullary sinuses (note that cortical sinuses are not pictured here). (A) Although high MW molecules were excluded from lymph node cortex and moved through the lymph node only via the sinuses, rapid movement of low MW molecules (B) from the subcapsular sinus to the HEVs was restricted to the fibers of the reticular network. (C) Comparison of the distribution in the lymph node of lymph-borne soluble molecules by size. SCS, subcapsular sinus; T, T cell area; B, B cell area, follicle; RF, reticular fiber; FRC, fibroblastic reticular cell; G, HEV endothelial glycocalyx; M, medulla.

fection. Vaccinia virus stocks (WR; $\sim 2 \times 10^8$ PFU/ml) were sonicated and $\sim 10^7$ PFU were injected into the rear footpads of normal female C57BL/6 mice (Taconic Farms) in 50 μl BSS/BSA. 8 h after injection of virus, at which point no observable inflammation at the site of injection had occurred, a combined solution of Texas red–labeled dextran (10 kD) and fluorescein-labeled dextran (70 kD), 5 mg/ml each, was injected into the rear footpads of both virus-injected and control mice. 5 min after dextran injection, the mice were killed by cervical dislocation and the popliteal lymph nodes were removed and immersion fixed.

Lymph Node Preparation and Sectioning

After excision, draining lymph nodes were immediately placed in freshly made 4% paraformaldehyde/0.1% glutaraldehyde in 10 mM morpholine propane sulfonic acid (MOPS)-buffered Ringer's solution (pH 7.4; room temperature for 1–2 h, then 4°C overnight). Fixed lymph nodes were washed in PBS for 30 min and blotted. Fixed or fresh lymph nodes were positioned in moulds filled with OCT (Baxter), then frozen in an isopentane/dry ice bath. Lymph nodes were sectioned (10 μm) on a Cryostat microtome. The orientation of the nodes in the moulds resulted in sections in a vertical plane in relation to the hilar blood vessels (36). This orientation of the nodes created the greatest number of sections in parallel to the reticular fibers in the lymph node cortex. Sections on slides were rehydrated in PBS and coverslipped with Fluormount (Southern Biotechnology Associates, Inc.).

Histochemistry and Immunocytochemistry

The reticular network in lymph node sections was stained using the Gomori reticulin stain (37), as detailed by Mallory (38), and the chemicals were obtained from Sigma-Aldrich.

To determine the relationship of B cells and HEL-FITC in lymph nodes after subcutaneous injections of HEL-FITC, lymph node sections were topically stained with anti–mouse CD45RA/B220–Cy-Chrome. In brief, fixed lymph node sections (10 μm) were dried on microscope slides for 1 h, then rehydrated and washed with PBS and PBS/0.1% BSA for 5 min each. The sections were incubated for 30 min with anti–CD45RA/B220–Cy-Chrome (1:100) in PBS/0.1% BSA, followed by three washes with PBS/0.1% BSA then PBS alone, and coverslipped.

To select lectins that label both lymphocytes and reticular network, a panel of lectins was studied on fresh-frozen sections of mouse lymph node. Sections were rehydrated, lectin applied, incubated for 30 min, washed three times, fixed, and coverslipped.

To examine the location of lymph-borne dextran in relation to the reticular fibers and fibroblastic reticular cells, fixed sections of draining lymph nodes, after a subcutaneous injection of Texas red–labeled dextran (10 kD), were topically labeled with the lectin, WGA-FITC (10 μg/ml). The sections were manipulated as described above for labeling with CD45RA/B220.

Controls included fresh-frozen or fixed-frozen lymph node sections as needed.

Microscopy and Image Processing

Reticulin stains of lymph node sections were examined using a ZEISS AxioPlan2 microscope, and differential interference contrast (DIC) images were obtained with a Spot-2 CCD camera. Micrographs of the location of HRP/diaminobenzidine reaction in relation to the reticular fibers were obtained by TEM (AEI 801 electron microscope; Philips). Images of the distribution of fluorophore-labeled molecules in lymph node sections were collected using the ZEISS 410 confocal laser scanning microscope. These images are compiled projections of 30–40 optical sections. Three-dimensional images were compiled and rotated using Imaris software.

Results

In General, Lymph-borne Molecules Do Not Percolate through Lymph Node Vortex. We have studied the distribution of a diverse set of fluorophore-labeled molecules in draining lymph nodes after subcutaneous injections in both rats and mice. Two distinct patterns of distribution of soluble, lymph-borne molecules in the lymph nodes were observed (Fig. 1). All fluorophore-labeled molecules reached the draining lymph node and could be seen in the subcapsular and medullary sinuses. The entry of soluble molecules from the subcapsular sinus into the cortex was dependent on

Table I. *Summary of Tracer Characteristics and Their Distribution in Lymph Node Cortex*

Soluble molecule	MW	MR	SCS	IC	Fiber	HEV	Ref.
	kD	*nm*					
Acridine orange	0.302	0.39	+	+			66
Dextran 3 kD –Fluor or –TR	3.0	1.01	+	±	+	+	67
LPS-FITC	3.4–100	1.07–4.29	+	−	−	−	40, 66
RANTES-Cy5	8.657	1.54	+	−	+	+	66, 68
MIP-1α–FITC	8.303	1.57	+	−	+	+	66, 68
IL-8–FITC	8.941	1.59	+	−	+	+	66, 68
HEL	14.3	1.93	+	−	+	+	39
α-Lactalbumin (bovine)	14.5	2.01	+	−	+	+	69
Dextran 10 kD –Fluor or –TR	10	2.22	+	−	+	+	70
OVA	48	2.73	+	±	+	+	70
HRP	38	3.02	+	±	+	+	71
WGA	43.2	3.04	+	−	+	±	66
PSA	46	3.12	+	−	+	±	66
LCA	50	3.23	+	−	+	±	66
BSA	68	3.6	+	−	+	+	72
Dextran 40 kD –Fluor or –TR	37–40	4.0–5.0	+	±	+	+	73
LPS-Fluor	3.4–100	1.07–4.29	+	−	−	−	40, 66
IgG	150	5.34	+	−	−	−	74
Dextran 70 kD –Fluor or –TR	70	5.5	+	−	−	−	75
Dextran 500 kD –Fluor	500	11.7	+	−	−	−	75
Dextran 2,000 kD –TR	2,000	16.0	+	−	−	−	75

SCS, subcapsular sinus; IC, intercellular, in the cortical parenchyma; Fiber, reticular fiber; Fluor, fluorescein; TR, Texas red. All other molecules labeled with FITC. Ref., reference(s).

molecular size. High MW molecules were undetectable within the cortex (Fig. 1 A). Conversely, low MW molecules highlighted the reticular network and HEVs in the T cell–dependent areas of the lymph node cortex (Fig. 1 B), whereas little fluorescence was detectable between lymphocytes in the T cell cortex. Fig. 1 C gives an overview of the effect of molecular size on distribution in the lymph node, and all molecules studied, with their distributions listed in order of their molecular size in Table I.

High MW Molecules Excluded from the Cortical Parenchyma of the Lymph Node. Fluorophore-labeled dextrans (3–2,000 kD) were used as soluble tracers to test the effect of size on soluble molecule distribution in the lymph node. The high MW dextrans, 2,000 and 500 kD (16- and 11.7-nm hydrodynamic radius [MR]; Table I), are similar in size to colloidal carbon (with molecular diameters reported as 20–70 nm [39], and 35–45 nm [22]). Like carbon, these dextrans were easily detectable in the subcapsular sinuses (Fig. 2 A, 500 kD shown) and medullary sinuses (not shown). This distribution was also typical for 70-kD dextran (5.5-nm MR; Fig. 3, A and B). However, all three of these differently sized dextrans were undetectable in the lymph node cortex.

IgG is similar in molecular size to 70-kD dextran (5.34- vs. 5.5-nm MR, respectively), yet it is globular in shape, unlike dextran, which has an extended conformation. The distribution of FITC-labeled mouse IgG was similar to 70-kD dextran in that it filled the subcapsular and medullary sinuses with minimal penetration into the cortex (not shown). To be certain of the distribution of IgG, both anti–mouse and anti–rat MHC class I antibodies were used as "cumulative" markers in mice and rats, respectively. Our intent was that if the anti–MHC class I antibodies gained access to the cortical parenchyma, they would bind any class I–bearing cell they came into contact with and therefore would be a record of access. The class I antibodies were easily detected in the subcapsular and medullary sinuses. However, in our studies, lymphocytes in the cortical microenvironments, which express class I molecules on their surfaces, were unlabeled with antibody, suggesting that lymph-borne antibody did not have access to the cortex (Fig. 2 B). These observations suggest the existence of a barrier that can limit percolation of both proteins and polysaccharides from lymph into the parenchyma of a draining lymph node.

Since LPS is a microbial product with profound effects on cellular immune responses, the accessibility of LPS to cells within the draining lymph node after administration in the footpad was studied. The monomeric form of LPS is 3.4 kD; therefore, the distribution might be expected to resemble that of low MW molecules. In fact, LPS-FITC was primarily detectable in the subcapsular and medullary sinuses, in a staining pattern similar to those observed after injection of high MW tracers (Fig. 2 C). This may be accounted for, in part, by physiological aggregation of LPS monomers into micelles with MW $>$ 100 kD (40). The exclusion of LPS is efficient but not always absolute. The image shown was chosen specifically to show a rare area of intercellular accumulation in the cortex below the subcapsular sinus.

Low MW Dextrans and Proteins Gained Access to the Cortex but Primarily Highlighted the Reticular Network and HEVs in the Interfollicular Regions. In contrast to the limited distribution of high MW molecules, low MW dextrans (3, 10, and 40 kD) arriving at the lymph node via lymphatics gained entry into the cortex, but only in a very defined manner. The dextrans highlighted distinct structures in the cortex (Fig. 3, A and B) that appeared identical to the reticular network stained by the Gomori silver stain for reticulin (Fig. 3 C). Note that both Gomori stain and dextrans highlight fibers that cross the subcapsular sinus, extend beyond the floor of the subcapsular sinus into the cortex, and connect to the HEVs. In addition, there are fibers that appear to begin at the floor of the subcapsular sinus and dive into

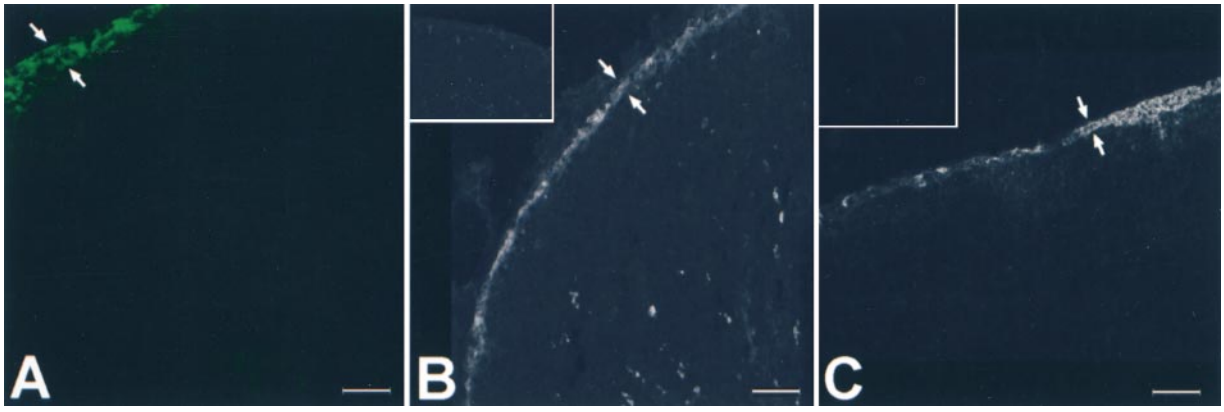

Figure 2. Exclusion of high MW molecules and LPS from lymph node cortex. Confocal micrographs showing subcapsular sinuses (between arrows) and underlying cortices of draining mouse lymph nodes after fluorophore-labeled molecules were injected subcutaneously. The lymph nodes were excised and immersion fixed within 10–12 min after injection. Lymph node sections, 10 μm thick. Bars, 50 μm. (A) Fluorescein-labeled dextran (500 kD, green) and Texas red–labeled dextran (2,000 kD, red) in a mouse axillary lymph node after footpad and intravenous injections, respectively. (B) Anti–mouse MHC class I–FITC (150 kD, white) in mouse lymph node. Inset shows control node; note the autofluorescent cells in both control and experimental conditions due to gain used (C). LPS-FITC (white) in mouse lymph node. Control node in inset.

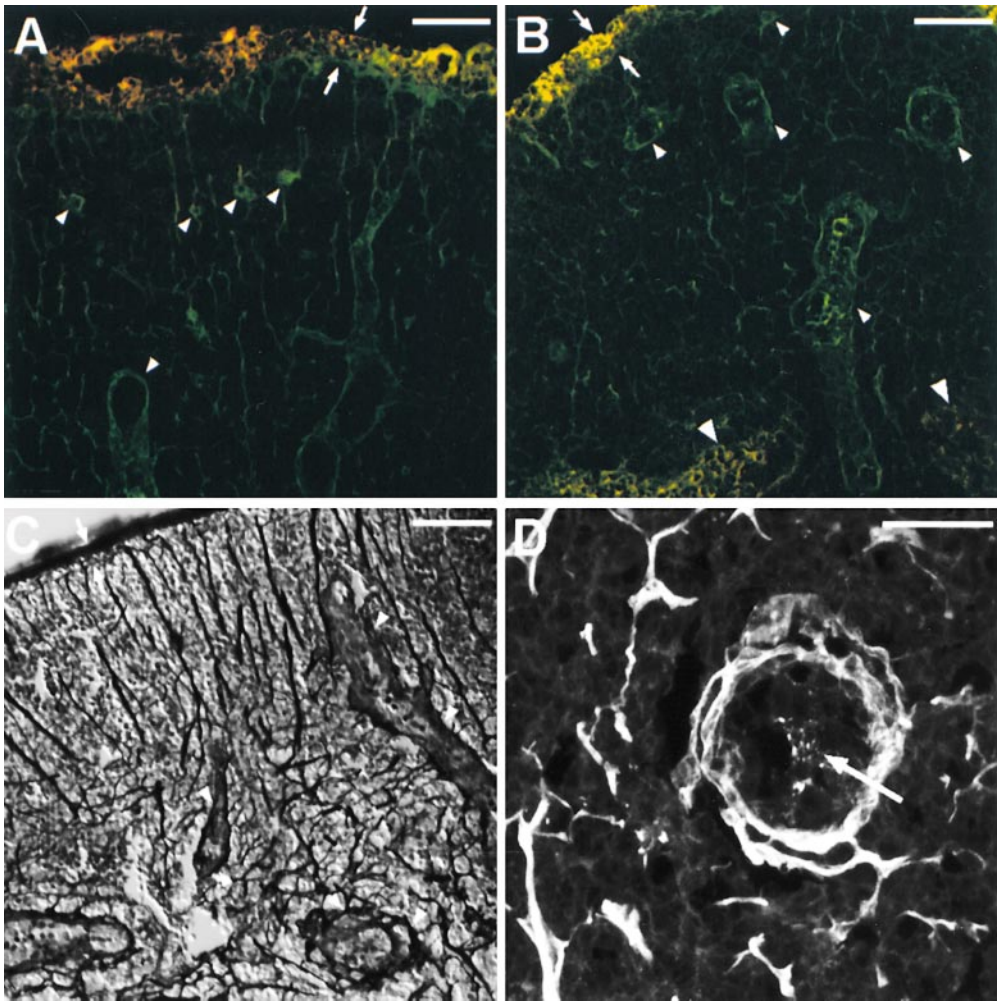

Figure 3. Low MW, soluble molecules enter lymph node cortex and distribute in a pattern resembling reticular network. Distribution of lymph-borne, fluorophore-labeled dextrans in draining rat and mouse lymph nodes is compared with Gomori silver staining of the reticular network in a mouse lymph node (confocal and bright-field micrographs, respectively). After the subcutaneous injection of dextrans, draining lymph nodes were excised and immersion fixed within 10–12 min. Lymph node sections are 10 μm thick. Subcapsular sinuses (between arrows) and typical HEVs (arrowheads) are labeled. (A) Fluorescein-labeled dextran (3 kD, green) and Texas red–labeled dextran (70 kD, red). (B) Fluorescein-labeled dextran (40 kD, green) and Texas red–labeled dextran (70 kD, red). (C) Gomori reticulin stain of mouse lymph node. (D) Higher magnification of HEVs in rat lymph node after subcutaneous injection of Texas red–labeled dextran (10 kD, white). Note the dextran in lumen (arrow). Bars, (A–C) 50 μm; (D) 25 μm.

the cortex and may also connect to HEVs. Texas red–labeled dextran (70 kD) was coadministered with the low MW dextrans and remained in the subcapsular sinus (yellow), indicating that 70-kD dextran exceeded a threshold for penetration into the parenchyma (Fig. 3, A and B). Subcutaneous injection of FITC-labeled dextran (70 kD) combined with Texas red–labeled dextrans (3 and 10 kD) resulted in a similar distribution, suggesting that charge was not an issue (data not shown). Upon examination at higher magnification (Fig. 3 D), fluorophore-labeled dextran (10 kD) appeared to trace an intricate woven pattern around the HEVs and continued between high endothelial cells and into the lumen itself. It is likely that the dextran is following the reticular fibers, which interweave with the extracellular matrix between the fibroblastic reticular cells that enwrap the HEVs and also with the basement membrane of the high endothelium (29, 41).

Fluorophore-labeled, low MW proteins distributed in the cortex like the low MW dextrans, primarily associated with the reticular network and HEVs (Table I). Fig. 4, A and B, show the distribution of the widely used immunogens, HEL and OVA, in mouse lymph node. Interestingly, unlike 70-kD dextran, 68-kD BSA highlighted fibers and HEVs in the cortex (not shown here [28]). However, despite the similarity in MW, the molecular radius of albumin is actually much smaller than 70-kD dextran (3.6 vs. 5.5 nm, respectively). Therefore, the barrier to entry into the lymph node cortex may be defined to a greater extent by molecular radius than by absolute MW.

Lectin Tracer Demonstrates Movement Is from Subcapsular Sinus towards HEVs. In these studies, we used fluorophore-labeled lectins with low MWs (Table I) to clarify two issues. First, the fluorescent signal of lymph-borne, low MW molecules was strongest in the subcapsular and medullary sinuses, followed by that in the fibers of the lymph node cortex. The arrival of the fluorophore by afferent lymphatic into the subcapsular sinus suggested that the direction of movement through the reticular network was in the direction from subcapsular sinus to HEV. However, most tracers in our hands distributed within the lymph node too rapidly to record the direction. As the reticular network spans between the subcapsular sinus and medullary sinus, we thought it was important to verify the source and direction of lymph-borne material through the network. Second, a dim fluorescence between lymphocytes in the cortical parenchyma was often visible, especially just below the floor

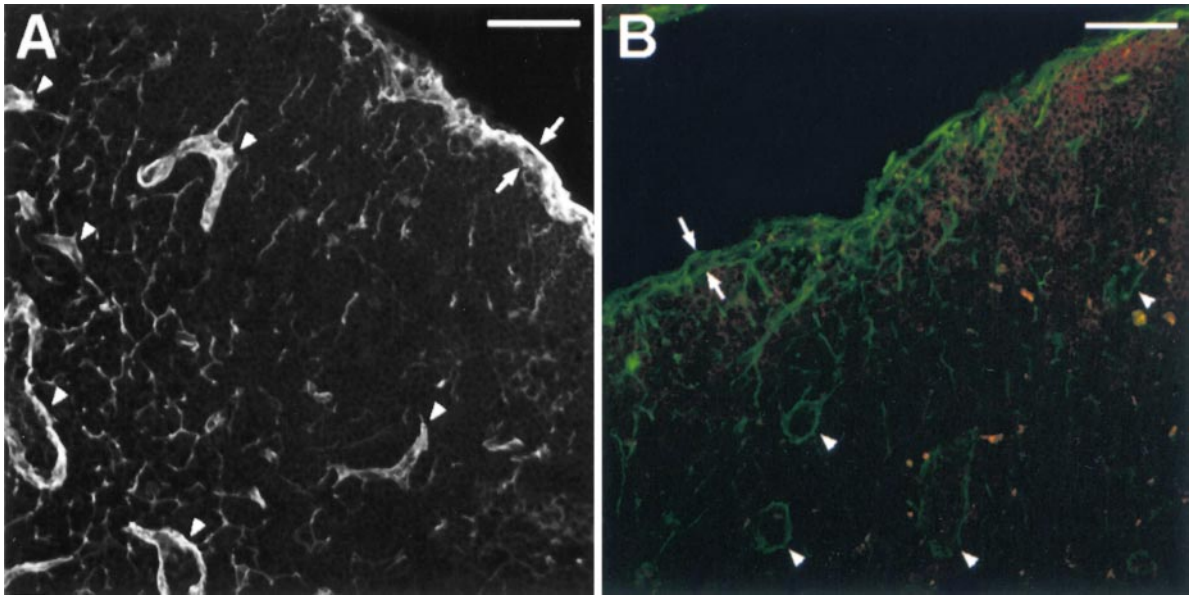

Figure 4. Typical protein immunogens have restricted distribution in cortices of draining lymph nodes after subcutaneous injection. Confocal micrographs of lymph node sections (10 μm) show FITC-labeled protein in subcapsular sinus (between arrows), highlighting reticular network and HEVs (arrowheads). Bars, 50 μm. (A) OVA-FITC (white) in the draining axillary lymph node. Lymph node was excised and fixed 15 min after injection of OVA into the mouse footpad. (B) HEL-FITC (green) in draining mouse lymph node. Lymph node was excised and fixed 5 min after injection of HEL into the footpad. Lymph node section was labeled topically with Cy-Chrome–labeled anti–mouse CD45R/B220 antibody to visualize B cells (red).

of the subcapsular sinus. To determine the extent of soluble molecule penetration into the lymphocyte environment, we wanted markers that would bind to the cells and be retained rather than be dependent on fixation of the markers in place. Lectins that bound both lymphocytes and the reticular network upon topical application on fresh-frozen lymph node sections included WGA, LCA, and PSA-FITC (Fig. 5 A). Therefore, these three lectins were studied as

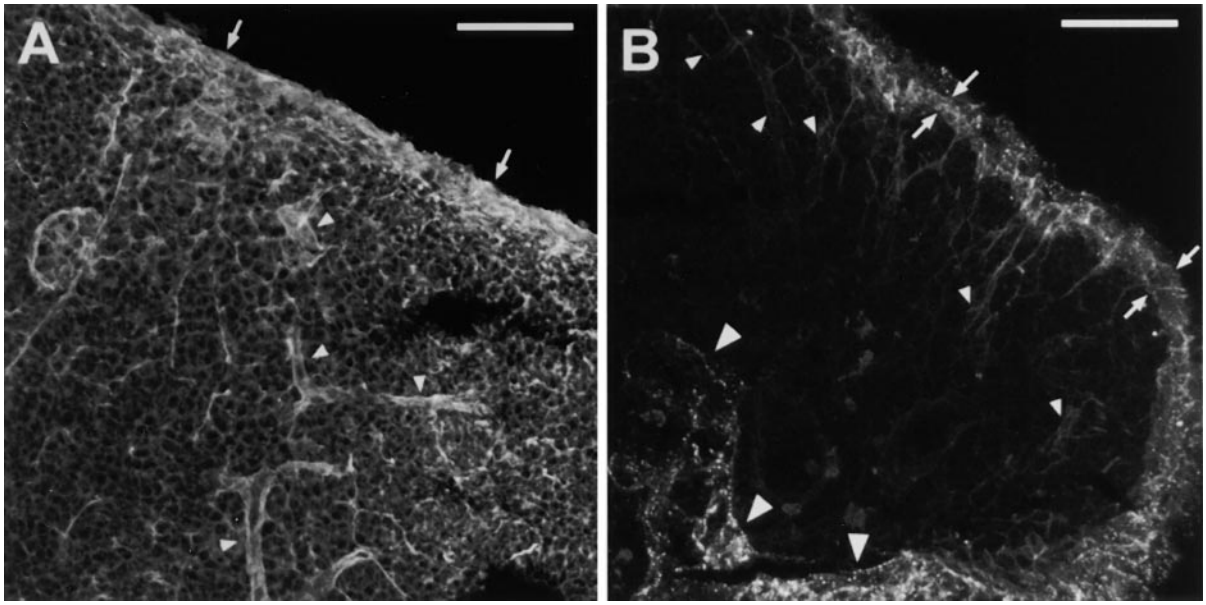

Figure 5. Lymph-borne molecules travel unidirectionally from the subcapsular sinus (arrows) through the reticular network toward HEVs (small arrowheads) in the lymph node cortex and are excluded from the lymphocyte microenvironments. Lymph node sections, 10 μm. Bars, 50 μm. (A) Lymphocytes, reticular fibers, and HEVs are visible in this confocal micrograph of a fresh-frozen section of mouse lymph node, topically labeled with FITC-labeled lectin, PSA (PSA-FITC). (B) Lymph-borne PSA-FITC highlights the subcapsular (arrows) and medullary (large arrowheads) sinuses and an incomplete reticular network starting at the subcapsular sinus. Small arrowheads point to three HEVs that are also highlighted by the lymph-borne PSA-FITC: two HEVs cut in cross-section (small arrowheads, middle right) and a single HEV with two branches, cut longitudinally (three small arrowheads, top left). Note the absence of labeled lymphocytes in the cortex. This draining lymph node was excised and fixed 30 min after injection of PSA-FITC into the footpad.

lymph tracers like the other molecules studied thus far. When administered via footpad, the distribution pattern of the lectins was distinctive and informative. Again, like the other low MW tracers, the fluorescence signal of FITC-labeled lectin was in the subcapsular and medullary sinuses as well as in fibers descending from the subcapsular sinus (PSA-FITC; Fig. 5 B). Intercellular fluorescence in the cortex was very low in intensity and only visible just below the subcapsular sinus for a distance of two to three cell diameters. There appeared to be no difference between the lymph nodes taken at 5 and 30 min after the subcutaneous injection in intensity or distance of penetration of the intercellular fluorescence. This confirmed that access of lymph-borne material to the lymphocytes of the cortical parenchyma was restricted.

FITC-labeled lectins filled both the subcapsular and medullary sinuses as well as highlighted fibers and HEVs near the floor of the subcapsular sinus. However, unlike other tracers, the fibers and HEVs in the deeper cortex were devoid of FITC-labeled lectin, regardless of whether the draining lymph nodes were removed 3 or 30 min after subcutaneous injections. Such partial penetration of the lectins implies a unidirectional movement of tracers within the reticular network from the subcapsular sinus to the HEVs.

Tracers Found within Reticular Fibers. To determine the relationship between tracer molecules and reticular fibers, lymph node sections were examined by confocal microscopy and TEM (Fig. 6, A–D). Fig. 6 A shows the distribution of 10-kD dextran (Texas red labeled) in a rat lymph node. Four large fibers (red) descend perpendicularly into the parenchyma from the floor of the subcapsular sinus (Fig. 6 A, top). These fibers intersect with a capillary that parallels the floor of the subcapsular sinus, showing intimate connectivity with the vascular system. In addition, the fibers are outlined by a fine green surface stain, FITC-labeled WGA, consistent with the expected fibroblastic reticular cell outline. In cross-section, both fibers appear filled with the Texas red–labeled dextran and are bounded by WGA, suggesting a reticular cell outline (Fig. 6 B). In Fig. 6 C, a fiber bounded by fibroblastic reticular cells courses diagonally across the image between two lymphocytes in a rat lymph node. Comparison of the electron density of the fiber to a fiber in a control lymph node from the same experiment demonstrates the abundance of HRP in the fiber after intralymphatic injection (Fig. 6, C and D). These studies indicate that lymph-borne material traffics through the reticular fibers.

Particulate Accumulation of High MW Tracer in Cortex after, Not during, the Initial Bolus of Soluble Tracer in Subcapsular Sinus. As shown previously, high MW dextran (green) administered subcutaneously arrived rapidly (<5 min) in the subcapsular and medullary sinuses and was not detectable in cortex (Fig. 7 A). To determine if the distribution changed, we extended our time sequence to 30 min and 4 h. At 30 min, the signal for dextran was noticeably lower in subcapsular sinus (compared with 5 min) but still high in medulla with no apparent signal in cortex (Fig. 7 B), consistent with transit of the majority of dextran through lymph node as a short-term bolus. At 4 h, the dextran (green) could be seen in both the subcapsular sinus and cortex but with altered characteristics (Fig. 7 D). There were high intensity particulate accumulations of dextran in both the subcapsular sinus and cortex, consistent with intracellular accumulation in phagocytic cells (e.g., dendritic cells and macrophages). For the 4-h time point, a low MW dextran (10 kD, Texas red, red) was injected subcutaneously, 10 min before lymph node removal for both contrast and frame of reference, as it has been shown to highlight the subcapsular and medullary sinuses and the reticular network (Fig. 7 D, red).

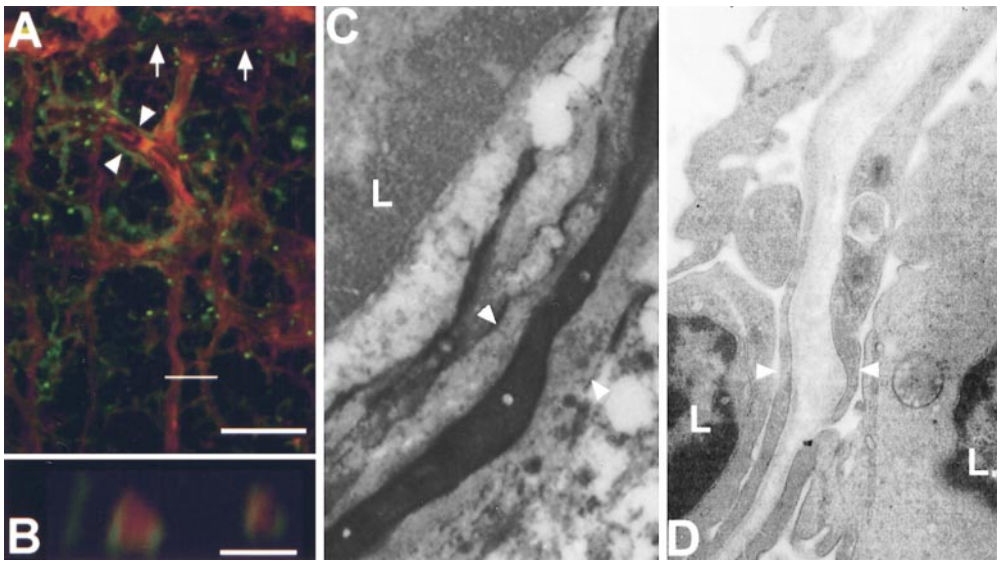

Figure 6. Lymph-borne, low MW molecules are in reticular fibers in the draining lymph nodes. (A) Confocal microscopy image of a draining rat mesenteric lymph node after the injection of Texas red–labeled dextran (10 kD, red) into the associated Peyer's patch. Reticular fibers (red) descend vertically from the dextran-filled subcapsular sinus (arrows). Topical application of the lymph node section with WGA-FITC (green) highlights cells associated with reticular network. A capillary intertwined by the reticular network runs horizontally across the image (arrowheads). Bar, 18 μm. (B) Optical cross-section of two reticular fibers at the white line in A. Note the Texas red–dextran encircled by WGA-FITC. Bar, 4 μm. (C and D) TEMs of reticular fibers ensheathed by fibroblastic reticular cells (arrowheads) in rat mesenteric lymph nodes. L, the nuclei of cortical lymphocytes. In C, the reticular fiber is filled with lymph-borne HRP; D is from the control of the same experiment.

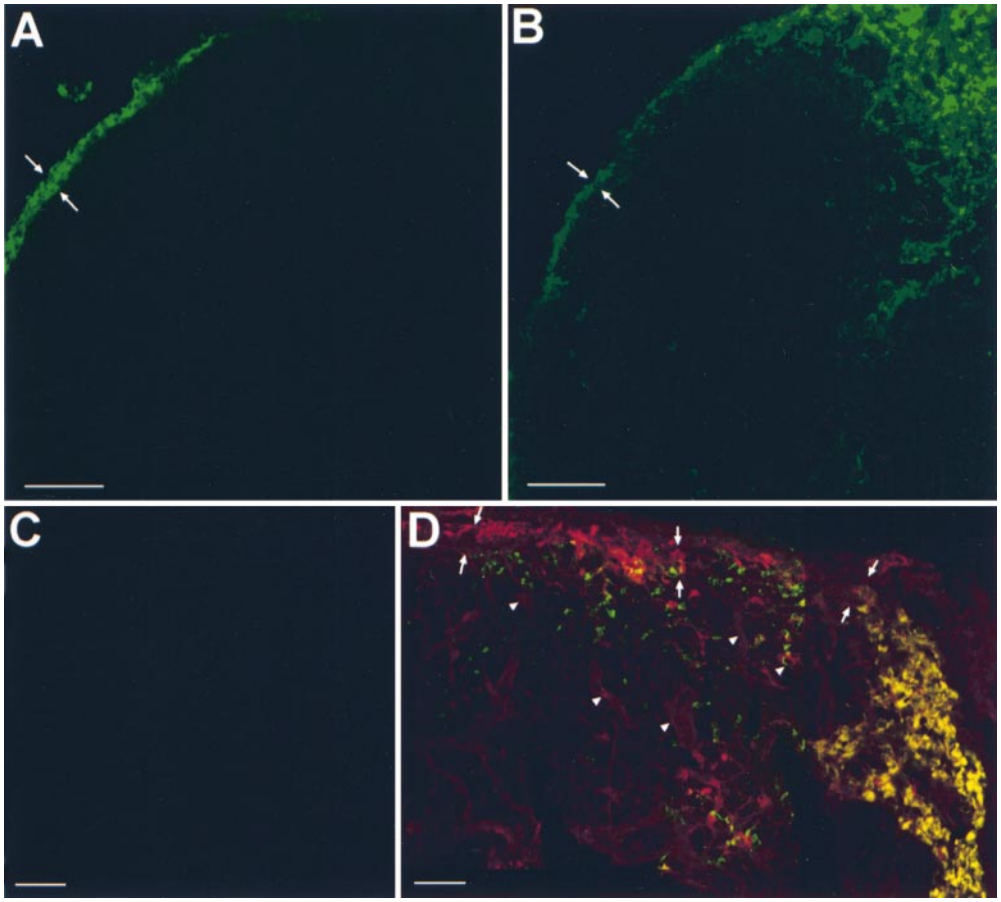

Figure 7. Particulate accumulation of high MW tracer in cortex after, not during, the initial bolus of soluble tracer in subcapsular sinus. (A) High MW dextran only in subcapsular sinus (arrows) at 5 min after subcutaneous injection. (B) At 30 min, lower intensity signal of high MW dextran in subcapsular sinus (arrows) but high persistent signal in medulla (on right). (C) Control lymph node. (D) Montage of adjacent areas of popliteal lymph node. Focal accumulation of high MW dextran (2,000 kD, fluorescein labeled, green) at 4 h within parenchyma contrasts with reticular-type distribution of low MW dextran (10 kD, Texas red, red) at 10 min (subcapsular sinus, arrows; HEV, arrowheads). However, despite different times of administration, both tracers coaccumulated in a cellular-type distribution within a medullary sinus. Bars, 50 μm.

Note that the particulate 4-h accumulated tracer in cortex (green) does not overlap with the 10-min accumulated tracer highlighting the reticular network (red). However, in medulla, the signals for both dextrans overlap (Fig. 7 D, yellow). Thus, medullary accumulation is consistent with acute uptake from the early bolus of soluble material, whereas cortical uptake is not. Instead, the lag between the original bolus (0 h) and cortical accumulation (4 h) suggests cortical accumulation is from another source, perhaps cellular uptake in tissue.

Rapid Enlargement of Lymph Node due to Viral Infection Had No Effect on Dextran Distribution. The distribution of dextrans and proteins in the lymph node indicated a functional barrier limiting entry of soluble molecules into the parenchyma. However, the lymph node is a dynamic lymphoid compartment, affected dramatically by inflammatory stimuli. To test whether inflammatory stimuli, such as those generated during infection, affected transport of lymph-borne solutes, we tested whether the barrier remained intact during a vaccinia virus infection. Vaccinia virus is a poxvirus known to induce both a large inflammatory response and a dramatic increase in the number of lymphocytes in the lymph node. The weights of lymph nodes, 8 h after injection of modified virus, increased by 41% over that of similar controls (1.2 ± 0.1, $n = 3$, and 1.7 ± 0.2, $n = 5$; mean $\pm$ SD), demonstrating a marked increase in size of the node. Yet distribution of dextrans was the same in lymph nodes from control animals (Fig. 8 A) and those infected with vaccinia virus (Fig. 8 B). Fluorescein-labeled dextran (70 kD) highlighted the sinuses but was excluded from the parenchyma, whereas Texas red–labeled dextran (10 kD) selectively decorated fibers and HEVs in draining lymph nodes. Therefore, the pattern of tracer distribution did not change, despite dramatic changes in lymph node size and cellularity during early viral infection.

Lymph-borne Chemokines Gained Access to HEVs via Reticular Network Conduits. After we had established the distribution of low MW molecules, e.g., dextran (10 kD), lactalbumin, and HEL, we could finally confront the enigma that prompted the initiation of these studies: the unexpected localization of chemokines (8–10 kD) on the luminal surface of the HEVs. Therefore, we studied the distribution of fluorophore-labeled chemokines following footpad injection. MIP-1α, IL-8, and RANTES (FITC and Cy5) each distributed in a similar pattern to the other low MW molecules. Fig. 9 illustrates results for MIP-1α–FITC, which was representative of the three chemokines. Fluorophore-labeled chemokine was visible in the subcapsular, cortical, and medullary sinuses. In the T cell–dependent areas, fluorophore-labeled chemokine was visible in the reticular network and around HEVs with little detectable chemokine intercellularly between lymphocytes. Thus, chemokines injected subcutaneously moved rapidly to the HEVs of the draining lymph node via the reticular network.

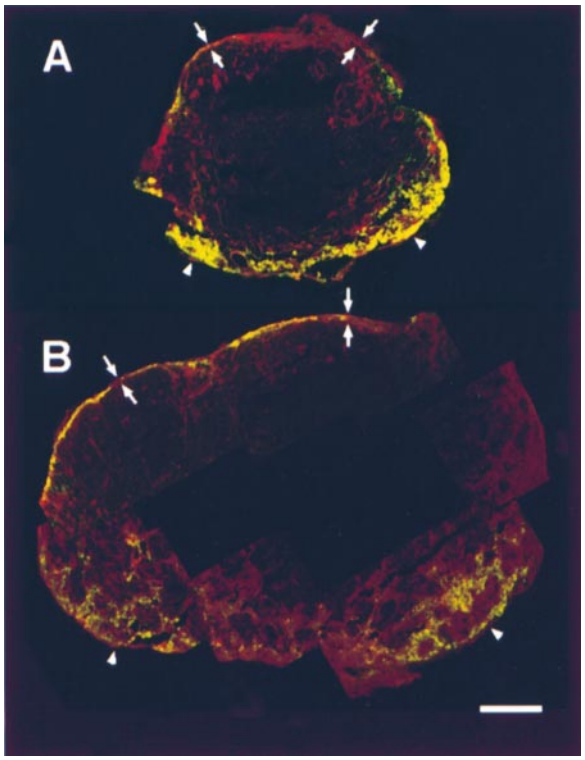

Figure 8. Despite acute changes in lymph node system during viral infection, patterns of distribution of lymph-borne, soluble molecules are preserved. Montages of confocal images of lymph node sections (10 μm) from control (A) and virally infected (B) draining mouse popliteal lymph nodes are presented here. Mouse popliteal lymph nodes were excised and immersion fixed 5 min after footpads were injected with fixable, fluorophore-labeled dextrans (10-kD dextran–Texas red [red], and 70-kD dextran–fluorescein [green]). Bar, 160 μm. (A) Control lymph node. (B) Virally infected lymph node, 8 h after footpad injection with modified vaccinia virus. Note that both low and high MW fluorophore-labeled dextrans filled the subcapsular (arrows) and medullary sinuses (arrowheads), whereas the lower MW dextran (red) highlights the reticular network and associated HEVs in the cortex of each lymph node.

Discussion

These studies have two distinct functional implications regarding the access and delivery of lymph-borne soluble molecules to the cortex of a draining lymph node. First, penetration of lymph-borne, soluble molecules into the cortical parenchyma, an area where T cell–APC interactions occur, is restricted. Second, low MW, lymph-borne, soluble molecules move rapidly through the lymph node cortex to the HEVs via a remarkable anatomic network, thus assuring access of chemokines and other soluble mediators to the HEVs.

It is generally accepted that lymph flows into the subcapsular sinus of the draining lymph node, through to the medullary sinus, and exits the lymph node at the hilum as efferent lymph. In addition, some studies suggest that a portion of lymph leaves the subcapsular sinus and percolates through the lymph node cortex (14, 16). Percolation is conceptually appealing, as it would assure access of soluble factors to lymphocytes and APCs, as well as stromal and other immune cells in the cortex, and therefore directly contribute to the immune response. The possibility of percolation is further supported by studies of the subcapsular sinus floor using electron microscopy. The physical structure across which soluble molecules would have to move is composed of extracellular matrix sandwiched between sinus endothelium on the floor of the sinus and fibroblastic reticular cells facing the cortex (23, 24). Some, but not other electron microscopic studies indicate pores or gaps in one or the other cell layers of the floor of the subcapsular sinus (23, 24, 26, 27, 42). Anatomic evidence notwithstanding, our functional data strongly indicated that there was a functional barrier that restricted "percolation" of soluble, lymph-borne molecules into the cortex.

The efficiency of the barrier depended on the size of the lymph-borne molecules. High MW tracers appeared to be virtually excluded (Fig. 2); as high MW tracer was abundant in subcapsular sinus but absent in adjacent cortex, this

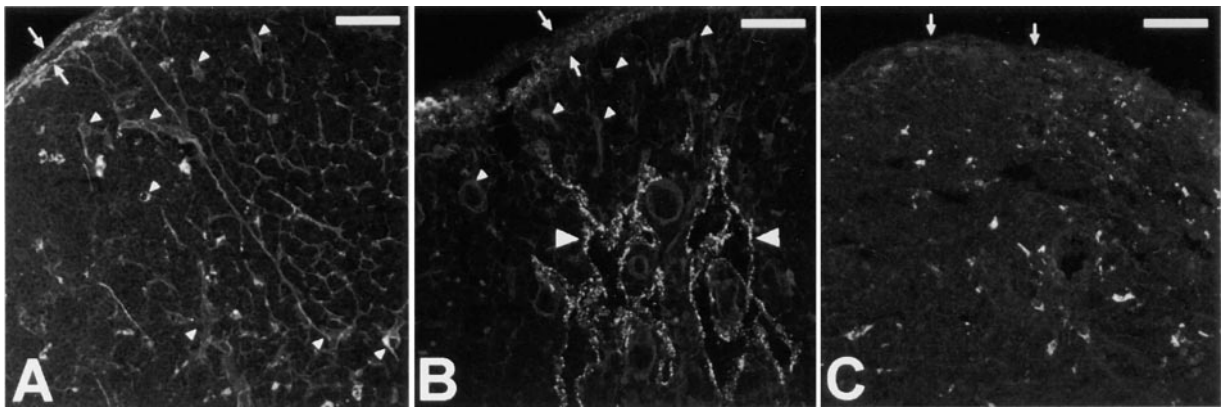

Figure 9. Lymph-borne chemokines travel to HEVs via reticular network "conduits." Confocal images shown of lymph-borne MIP-1α–FITC in subcapsular sinus (arrows), cortical/medullary sinuses (large arrowheads), and reticular fibers descending from the subcapsular sinus floor to several HEVs (small arrowheads) in a draining mouse axillary lymph node. The lymph node was excised and immersion fixed 15 min after subcutaneous injection of the chemokine into the footpad. (A) Cortex. (B) Cortical/medullary sinuses (large arrowheads). (C) Control showing autofluorescent cells due to gain used. Bars, 50 μm.

demonstrated that the floor of the subcapsular sinus that separates subcapsular sinus from cortex was an efficient functional barrier for high MW material. In contrast, for low MW tracers the exclusion was partial, not absolute. Specifically, there was detectable tracer in the cortex, on occasion, seen as faint outlining of lymphocytes within the parenchyma (e.g., Figs. 3 and 4). That signal, when observed, was at a level several-fold weaker than adjacent subcapsular sinus or reticular network; any detectable cortical signal was generally evident subjacent to the subcapsular sinus with less or no signal in the deep cortex. A limit to the protection of the cortical parenchyma by this functional barrier is demonstrated by the free movement of very small molecules such as tritiated uridine (~350 daltons; reference 43) and acridine orange (302 daltons; our data not shown) throughout the cortex.

Restricted access of lymph-borne material to cortical parenchyma would not only preserve the milieu of lymphocyte microenvironments, but also protect the lymphocytes from a potentially varied collection of lymph-borne substances. This would be especially advantageous with those substances that would adversely influence an immune response occurring within the cortex. For example, during microbial infections, this barrier may be important for exclusion not only of the microbes themselves, but also of their soluble products, which can perturb immune responses. Our findings of microbial LPS in the subcapsular and medullary sinuses, rather than in the cortex, illustrated such exclusion. The adaptability of the lymph node and this functional barrier became evident during an induced viral infection with vaccinia virus. The increase in lymph node weights 8 h after injection of vaccinia virus, compared with similar controls, suggested that the surface area of the floor of the subcapsular sinus had increased by ~30%. However, the distribution of fluorophore-labeled dextrans did not change, demonstrating that this functional boundary remained intact even in the event of acute enlargement of the lymph node during viral infection. Thus, this functional barrier may isolate the cortex from a potentially varied collection of substances, which would impair the immunological response. On the other hand, this functional barrier will limit the ability of APCs already in the cortex to acquire lymph-borne antigen. The timing and pattern of accumulation of high MW tracer within cortex (Fig. 7) fits the interpretation that delayed (4 h) appearance of tracer in cortex may be due to cellular uptake in the periphery rather than cellular uptake in the draining lymph node. The attenuation of uptake of low MW molecules by cortical-resident APCs will be quantitative not qualitative, as the restriction of tracer entry is relative and not absolute; consequently, its relevance would be greatest for immune challenges in which antigen concentration is limited.

Existence of the barrier discussed above poses a problem, as it would restrict access of lymph-borne material to HEVs, which are all located exclusively within the cortex. Nevertheless, even with this barrier in place, soluble tracers find their way to the HEVs. Previous studies show that rather than the diffuse distribution of soluble molecules as expected for percolation through the cortex, the proteins BSA-FITC, HRP, and Ig-FITC highlight the reticular network and HEVs in the cortex (22, 28). In our studies, we found that in addition to HRP and BSA-FITC, several other molecules comparable in size distributed in a similar fashion (Table I). However, in our results, IgG-FITC remained in the sinuses in both rats and mice, much like dextran (70 kD), suggesting that molecules above a certain threshold in size are excluded from not only the lymphocyte environment but also the reticular network. The cutoff for access to the reticular network was a molecular diameter between 7.2 and 10.7 nm, as demonstrated by the respective distributions of BSA and IgG. Preferential access to the reticular network relative to the lymphocyte environment continued to be demonstrated with smaller molecules, such as α-lactalbumin, 3-kD dextran (4- and ~2-nm molecular diameter, respectively), and chemokines.

The direction of flow of lymph through the lymph nodes of rats and mice is from the afferent lymphatics into the lymph node subcapsular sinus, and from there through the medullary sinus and out through the efferent lymphatic vessel. Therefore, it was logical that the direction of movement of lymph-borne material through the reticular network would be from subcapsular sinus to HEVs (28). However, the reticular fibers often extend from there to the medullary sinus; therefore the medullary sinus could, in theory, be a source of lymph for passage through the reticular network. Sainte-Marie and Peng (28) show a gradient of BSA from subcapsular sinus to HEVs. We confirmed that the direction of movement of lymph-borne material was from subcapsular sinus towards HEVs through the reticular network by using FITC-labeled lectins as lymph-borne tracers. The penetration of the lectins through the network was never as complete as other proteins, regardless of whether the draining lymph node was removed 3 or 30 min after subcutaneous injection. Nonetheless, the penetration through the reticular network always started at the subcapsular sinus despite the presence of lectin in the medullary sinus. The limited movement of the lectins through the reticular network may be due to interactions with proteoglycans and glycosaminoglycans (GAGs) associated with the collagens of the reticular network (44).

The movement of tracer molecules through the conduits is most consistent with bulk flow of water and tracers via the conduits. It is remarkable that bulk flow occurs along conduits, given that the hydrostatic pressure is low in afferent lymph, and that there is little resistance to its outflow via sinuses to the efferent lymphatics. These considerations argue that there must be special mechanisms which give rise to the transport observed. Three kinds of special mechanisms may be involved. (a) Active transport at the floor of the subcapsular sinus. Compton and Raviola (45) noted that there is an extraordinary abundance of vesicles in the sinus lining cells, so much so that a role in transport was considered but discounted because no transport across this barrier was expected. (b) Pressure source from fenestrated capillaries. Fenestrated capillaries intersect with reticular fibers just below the floor of the subcapsular sinus. Intravas-

cular injections of HRP have been shown to enter the reticular network with a decreasing gradient extending from these sites (22). Thus, fenestrations could allow fluid movement from the capillary into the conduit, providing additional hydrostatic pressure to drive flow towards the lower pressure in the venous system. (c) Active transport at the site of HEV outflow. Antal Rot and coworkers (46, 47) have demonstrated vesicular transport of chemokine from the abluminal to luminal surface of the venular endothelium. A combination of these three mechanisms probably gives rise to the tracer movement observed. Fluid volume transported by vesicle traffic would probably be insufficient to account for the observed rate of flow via the conduits. However, vesicular transport of tracer, coupled with bulk flow driven by fenestrated capillaries, might be sufficient.

Fluid movement along collagen fibers occurs in the interstitium of other tissues (48–53). Reticular fibers in the lymph node are distinctive in that each fiber is ensheathed by fibroblastic reticular cells (30). Therefore, each fiber is in an extracellular space distinct from the interstitial space of the parenchyma and continuous with the fibers in the floor of the subcapsular sinus and those enwrapping the HEVs (23, 29). Both Rinehart (54) and Moe (23) hypothesized that fluid movement might be directed along these fibers. Anderson and Anderson (22) and Sainte-Marie and Peng (28) showed preferential localization of several tracers along reticular fibers in rat lymph nodes between the subcapsular sinus and the HEVs, which are confirmed here. By extending the studies into the mouse with a wider range of tracers, we have revealed that molecular size was a factor in the access of lymph-borne soluble molecules to the reticular network. Both confocal microscopy and TEM confirmed that the tracer was localized within the reticular fiber rather than outside the ensheathing fibroblastic reticular cell. Thus, fluid movement within the reticular network in lymph node is a special case of the more general biological strategy of fluid movement along collagen fibers.

These findings may also have implications for B cell acquisition of antigen in lymph nodes. At the HEVs, low MW lymph-borne material arriving via the reticular network filled the perivenular channel and interendothelial spaces, i.e., between the endothelium and the layers of fibroblastic reticular cells enwrapping the HEVs and between the high endothelial cells. Incoming lymphocytes migrate through these spaces on their way from the HEV lumen to the cortical parenchyma. At this point, lymphocytes are bathed in the low MW lymph-borne molecules that arrive via the reticular network. This may then be a site where antigen-specific B cells could capture their soluble antigen and carry it with them into the cortex for presentation to T cells. In this context, it may be noteworthy that most "model antigens" like HEL and OVA are small enough to move through the reticular network to the HEVs.

Soluble mediators appear to be important for the phenotype of HEVs and the migratory events that occur there. SLC expressed by high endothelium promotes adhesion and chemotaxis of lymphocytes in lymph nodes (8, 55, 56). In addition, the specificity of chemokines for leukocyte subpopulations suggests that chemokines immobilized on endothelial glycocalyx may be involved in selective recruitment of leukocytes at postcapillary venules in general, and HEVs in particular (4, 57–59). An additional layer of selectivity and specificity lies with the interaction of chemokines to GAG subgroups in the endothelial glycocalyx or extracellular matrix (60–63). Therefore, the endothelial expression of GAGs luminally and abluminally plays an additional role in leukocyte recruitment. The access for chemokines draining from insulted tissue to the HEVs via the reticular network provides a means for additional recruitment. In addition, onset of such affects would occur rapidly after such soluble molecules were released from the draining tissue, but could be sustained as long as such molecules were being released. Moreover, inflammatory cytokines such as IL-1, TNF, and IFN-γ, which regulate intermediate and long-term endothelial phenotype (e.g., their expression of intracellular adhesion molecule [ICAM]-1 and vascular cell adhesion molecule [VCAM]-1 involved in leukocyte recruitment), could also reach the HEVs via this route (64, 65).

Our studies showed that chemokines travel through the reticular network to HEVs, thus providing an explanation for chemokine on the luminal surface of an HEV that does not produce it (4, 8). A diverse group of molecules are likely to travel to HEVs via this route in vivo, including a variety of soluble mediators that could be physiologically important both abluminally and luminally at the HEVs. Therefore, the reticular network is positioned to play an important role in the orchestration of lymphocyte recirculation and immune responses by acting as a conduit for the delivery of small, lymph-borne molecules, including antigens and chemokines, from subcapsular sinus to HEVs.

We thank T. Brotz for the use of the Experimental Immunology Branch Microscopy and Digital Imaging Facility; and Eric Kaldjian, Tilmann Brotz, Jack Bennink, Jon Yewdell, Caetano Reis e Sousa, Claire Chougnet, and Martin Brown for useful discussions. We thank R.E. Offord and B. Dufour for the synthesis of the fluorophore-labeled chemokines.

C.C. Norbury is the recipient of a Wellcome Prize Travelling Fellowship.

Submitted: 31 May 2000
Revised: 6 September 2000
Accepted: 23 September 2000

References

1. Gowans, J.L., and E.J. Knight. 1964. The route of re-circulation of lymphocytes in rat. *Proc. R. Soc. Lond. Ser. B.* 159: 257–282.
2. Butcher, E.C. 1991. Leukocyte-endothelial cell recognition: three (or more) steps to specificity and diversity. *Cell.* 67: 1033–1036.
3. Shimizu, Y., W. Newman, Y. Tanaka, and S. Shaw. 1992. Lymphocyte interactions with endothelial cells. *Immunol. Today.* 13:106–112.
4. Tanaka, Y., D.H. Adams, S. Hubscher, H. Hirano, U. Siebenlist, and S. Shaw. 1993. T-cell adhesion induced by pro-

teoglycan-immobilized cytokine MIP-1 beta. *Nature.* 361: 79–82.
5. Tedla, N., P. Palladinetti, M. Kelly, R.K. Kumar, N. DiGirolamo, U. Chattophadhay, B. Cooke, P. Truskett, J. Dwyer, D. Wakefield, and A. Lloyd. 1996. Chemokines and T lymphocyte recruitment to lymph nodes in HIV infection. *Am. J. Pathol.* 148:1367–1373.
6. Tedla, N., H.W. Wang, H.P. McNeil, N. Di Girolamo, T. Hampartzoumian, D. Wakefield, and A. Lloyd. 1998. Regulation of T lymphocyte trafficking into lymph nodes during an immune response by the chemokines macrophage inflammatory protein (MIP)-1 alpha and MIP-1 beta. *J. Immunol.* 161:5663–5672.
7. Ebnet, K., M.M. Simon, and S. Shaw. 1996. Regulation of chemokine gene expression in human endothelial cells by proinflammatory cytokines and *Borrelia burgdorferi*. *Ann. NY Acad. Sci.* 797:107–117.
8. Stein, J.V., A. Rot, Y. Luo, M. Narasimhaswamy, H. Nakano, M.D. Gunn, A. Matsuzawa, E.J. Quackenbush, M.E. Dorf, and U.H. von Andrian. 2000. The CC chemokine thymus-derived chemotactic agent 4 (TCA-4, secondary lymphoid tissue chemokine, 6Ckine, exodus-2) triggers lymphocyte function–associated antigen 1–mediated arrest of rolling T lymphocytes in peripheral lymph node high endothelial venules. *J. Exp. Med.* 191:61–76.
9. Larsen, C.G., A.O. Anderson, E. Appella, J.J. Oppenheim, and K. Matsushima. 1989. The neutrophil-activating protein (NAP-1) is also chemotactic for T lymphocytes. *Science.* 243: 1464–1466.
10. Hendriks, H.R., and I.L. Eestermans. 1983. Disappearance and reappearance of high endothelial venules and immigrating lymphocytes in lymph nodes deprived of afferent lymphatic vessels: a possible regulatory role of macrophages in lymphocyte migration. *Eur. J. Immunol.* 13:663–669.
11. Hendriks, H.R., A.M. Duijvestijn, and G. Kraal. 1987. Rapid decrease in lymphocyte adherence to high endothelial venules in lymph nodes deprived of afferent lymphatic vessels. *Eur. J. Immunol.* 17:1691–1695.
12. Mebius, R.E., D. Dowbenko, A. Williams, C. Fennie, L.A. Lasky, and S. R. Watson. 1993. Expression of GlyCAM-1, an endothelial ligand for L-selectin, is affected by afferent lymphatic flow. *J. Immunol.* 151:6769–6776.
13. Drayson, M.T., and W.L. Ford. 1984. Afferent lymph and lymph borne cells: their influence on lymph node function. *Immunobiology.* 168:362–379.
14. Nordmann, M. 1928. Studien an lymphknoten bei akuten und chronischen allgemeininfektionen. *Virchows Arch. Pathol. Anat.* 267:158–207.
15. Drinker, C.K., G.B. Wislocki, and M.E. Field. 1933. The structure of the sinuses in the lymph nodes. *Anat. Rec.* 56: 261–273.
16. Drinker, C.K., M.E. Field, and H.K. Ward. 1934. The filtering capacity of lymph nodes. *J. Exp. Med.* 59:393–406.
17. Hill, A.G.S., H.W. Deane, and A.H. Coons. 1950. Localization of antigen in tissue cells. V. Capsular polysaccharide of Friedlander bacillus, type B, in the mouse. *J. Exp. Med.* 92: 35–44.
18. Nossal, G.J., A. Abbot, J. Mitchell, and Z. Lummus. 1968. Antigens in immunity. XV. Ultrastructural features of antigen capture in primary and secondary lymphoid follicles. *J. Exp. Med.* 127:277–290.
19. Fukuda, J. 1968. Studies on the vascular architecture and the fluid exchange in the rabbit popliteal lymph node. *Keio J. Med.* 17:53–70.
20. Sainte-Marie, G., F.S. Peng, and C. Belisle. 1982. Overall architecture and pattern of lymph flow in the rat lymph node. *Am. J. Anat.* 164:275–309.
21. Fossum, S. 1980. The architecture of rat lymph nodes. IV. Distribution of ferritin and colloidal carbon in the draining lymph nodes after foot-pad injection. *Scand. J. Immunol.* 12: 433–441.
22. Anderson, A.O., and N.D. Anderson. 1975. Studies on the structure and permeability of the microvasculature in normal rat lymph nodes. *Am. J. Pathol.* 80:387–418.
23. Moe, R.E. 1963. Fine structures of the reticulum and sinuses of lymph nodes. *Am. J. Anat.* 112:311–335.
24. Clark, S.L.J. 1962. The reticulum of lymph nodes in mice studied with the electron microscope. *Am. J. Anat.* 110:217–257.
25. Forkert, P.G., J.A. Thliveris, and F.D. Bertalanffy. 1977. Structure of sinuses in the human lymph node. *Cell Tissue Res.* 183:115–130.
26. van Ewijk, W., P.J.M. Brekelmans, R. Jacobs, and E. Wisse. 1988. Lymphoid microenvironments in the thymus and lymph node. *Scanning Microsc.* 2:2129–2140.
27. Farr, A.G., Y. Cho, and P.P. De Bruyn. 1980. The structure of the sinus wall of the lymph node relative to its endocytic properties and transmural cell passage. *Am. J. Anat.* 157:265–284.
28. Sainte-Marie, G., and F.S. Peng. 1986. Diffusion of a lymph-carried antigen in the fiber network of the lymph node of the rat. *Cell Tissue Res.* 245:481–486.
29. Ushiki, T., O. Ohtani, and K. Abe. 1995. Scanning electron microscopic studies of reticular framework in the rat mesenteric lymph node. *Anat. Rec.* 241:113–122.
30. Hayakawa, M., M. Kobayashi, and T. Hoshino. 1988. Direct contact between reticular fibers and migratory cells in the paracortex of mouse lymph nodes: a morphological and quantitative study. *Arch. Histol. Cytol.* 51:233–240.
31. Anderson, A.O., and N.D. Anderson. 1976. Lymphocyte emigration from high endothelial venules in rat lymph nodes. *Immunology.* 31:731–748.
32. Anderson, A.O., and S. Shaw. 1993. T cell adhesion to endothelium: the FRC conduit system and other anatomic and molecular features which facilitate the adhesion cascade in lymph node. *Semin. Immunol.* 5:271–282.
33. Gretz, J.E., E.P. Kaldjian, A.O. Anderson, and S. Shaw. 1996. Sophisticated strategies for information encounter in the lymph node: the reticular network as a conduit of soluble information and a highway for cell traffic. *J. Immunol.* 157: 495–499.
34. Gretz, J.E., A.O. Anderson, and S. Shaw. 1997. Cords, channels, corridors and conduits: critical architectural elements facilitating cell interactions in the lymph node cortex. *Immunol. Rev.* 156:11–24.
35. Offord, R.E., H.F. Gaertner, T.N. Wells, and A.E. Proudfoot. 1997. Synthesis and evaluation of fluorescent chemokines labeled at the amino terminal. *Methods Enzymol.* 287: 348–369.
36. Kowala, M.C., and G.I. Schoefl. 1986. The popliteal lymph node of the mouse: internal architecture, vascular distribution and lymphatic supply. *J. Anat.* 148:25–46.
37. Gomori, G. 1937. Silver impregnation of reticulum in paraffin sections. *Am. J. Pathol.* 8:993–1001.
38. Mallory, F.B. 1968. Pathological Technique. Hafner Publishing Company, New York.

39. Algvere, P., and B. Martini. 1985. Sequelae of intravitreal phagocytic activity in response to microparticles. *Acta Ophthalmol. Suppl.* 173:107–110.
40. Skelly, R.R., P. Munkenbeck, and D.C. Morrison. 1979. Stimulation of T-independent antibody responses by hapten-lipopolysaccharides without repeating polymeric structure. *Infect. Immun.* 23:287–293.
41. Anderson, N.D., A.O. Anderson, and R.G. Wyllie. 1976. Specialized structure and metabolic activities of high endothelial venules in rat lymphatic tissues. *Immunology.* 31:455–473.
42. Racz, P., K. Tenner-Racz, Q.N. Myrvik, and J.R. Ockers. 1978. The "mosaic" structure of the sinuses in the hilar lymph node complex of the lungs in rabbits undergoing a pulmonary cell-mediated reaction: an electron microscopic study. *J. Reticuloendothel. Soc.* 24:527–545.
43. Sainte-Marie, G., and F.S. Peng. 1982. Distribution of a diffusible tracer in the subcapsular sinus and the cortex of lymph nodes in the rat. *Rev. Can. Biol. Exp.* 41:201–208.
44. Kramer, R.H., S.D. Rosen, and K.A. McDonald. 1988. Basement-membrane components associated with the extracellular matrix of the lymph node. *Cell Tissue Res.* 252:367–375.
45. Compton, C.C., and E. Raviola. 1985. Structure of the sinus-lining cells in the popliteal lymph node of the rabbit. *Anat. Rec.* 212:408–423.
46. Middleton, J., S. Neil, J. Wintle, I. Clark-Lewis, H. Moore, C. Lam, M. Auer, E. Hub, and A. Rot. 1997. Transcytosis and surface presentation of IL-8 by venular endothelial cells. *Cell.* 91:385–395.
47. Rot, A., E. Hub, J. Middleton, F. Pons, C. Rabeck, K. Thierer, J. Wintle, B. Wolff, M. Zsak, and P. Dukor. 1996. Some aspects of IL-8 pathophysiology. III: Chemokine interaction with endothelial cells. *J. Leukoc. Biol.* 59:39–44.
48. Kotani, M. 1990. The lymphatics and lymphoreticular tissues in relation to the action of sex hormones. *Arch. Histol. Cytol.* 53(Suppl.):1–76.
49. Guyton, A.C., and J.E. Hall. 1996. The microcirculation and the lymphatic system: capillary fluid exchange, interstitial fluid, and lymph flow. *In* Textbook of Medical Physiology. W.B. Saunders Company, Philadelphia. 1148 pp.
50. Fraley, E.E., and L. Weiss. 1959. An electron microscopic study of transport in the connective tissue and lymphatic capillaries of the rat diaphragm. *Anat. Rec.* 133:381 (Abstr.).
51. Schroer, H., and G. Hauck. 1977. Fluid and substance pathway through the extravascular space. *Bibl. Anat.* 15:231–233.
52. Hauck, G. 1985. Prelymphatic pathways. *In* The Initial Lymphatics. A. Bollinger, H. Partsch, and J.H.N. Wolfe, editors. George Thieme Verlag, Stuttgart. 220 pp.
53. Witte, S. 1984. The role of blood coagulation in capillary permeability Vitalmicroscopic contributions. *Biorheology.* 21: 121–133.
54. Rinehart, J. 1930. Reticulum. Its origin. The occurrence of reticulum fibrils in capillary endothelium. A new method of demonstration. I. The finer capillary bed. *Am. J. Pathol.* 6:525–539.
55. Gunn, M.D., K. Tangemann, C. Tam, J.G. Cyster, S.D. Rosen, and L.T. Williams. 1998. A chemokine expressed in lymphoid high endothelial venules promotes the adhesion and chemotaxis of naive T lymphocytes. *Proc. Natl. Acad. Sci. USA.* 95:258–263.
56. Nagira, M., T. Imai, R. Yoshida, S. Takagi, M. Iwasaki, M. Baba, Y. Tabira, J. Akagi, H. Nomiyama, and O. Yoshie. 1998. A lymphocyte-specific CC chemokine, secondary lymphoid tissue chemokine (SLC), is a highly efficient chemoattractant for B cells and activated T cells. *Eur. J. Immunol.* 28:1516–1523.
57. Rot, A. 1992. Endothelial cell binding of NAP-1/IL-8: role in neutrophil emigration. *Immunol. Today.* 13:291–294.
58. Tanaka, Y., D.H. Adams, and S. Shaw. 1993. Proteoglycans on endothelial cells present adhesion-inducing cytokines to leukocytes. *Immunol. Today.* 14:111–115.
59. Tanaka, Y., K. Fujii, S. Hubscher, M. Aso, A. Takazawa, K. Saito, T. Ota, and S. Eto. 1998. Heparan sulfate proteoglycan on endothelium efficiently induces integrin-mediated T cell adhesion by immobilizing chemokines in patients with rheumatoid synovitis. *Arthritis Rheum.* 41:1365–1377.
60. Witt, D.P., and A.D. Lander. 1994. Differential binding of chemokines to glycosaminoglycan subpopulations. *Curr. Biol.* 4:394–400.
61. Hoogewerf, A.J., G.S. Kuschert, A.E. Proudfoot, F. Borlat, I. Clark-Lewis, C.A. Power, and T.N. Wells. 1997. Glycosaminoglycans mediate cell surface oligomerization of chemokines. *Biochemistry.* 36:13570–13578.
62. Carr, M.W., R. Alon, and T.A. Springer. 1996. The C-C chemokine MCP-1 differentially modulates the avidity of beta 1 and beta 2 integrins on T lymphocytes. *Immunity.* 4:179–187.
63. Kuschert, G.S., F. Coulin, C.A. Power, A.E. Proudfoot, R.E. Hubbard, A.J. Hoogewerf, and T.N. Wells. 1999. Glycosaminoglycans interact selectively with chemokines and modulate receptor binding and cellular responses. *Biochemistry.* 38:12959–12968.
64. Strieter, R.M., S.L. Kunkel, H.J. Showell, D.G. Remick, S.H. Phan, P.A. Ward, and R.M. Marks. 1989. Endothelial cell gene expression of a neutrophil chemotactic factor by TNF-alpha, LPS, and IL-1 beta. *Science.* 243:1467–1469.
65. Thornhill, M.H., S.M. Wellicome, D.L. Mahiouz, J.S. Lanchbury, U. Kyan-Aung, and D.O. Haskard. 1991. Tumor necrosis factor combines with IL-4 or IFN-gamma to selectively enhance endothelial cell adhesiveness for T cells. The contribution of vascular cell adhesion molecule-1-dependent and -independent binding mechanisms. *J. Immunol.* 146:592–598.
66. Claes, P., M. Dunford, A. Kenney, and P. Vardy. 1992. An on-line dynamic light scattering instrument for macromolecular characterization. *In* Laser Light Scattering in Biochemistry. S.E. Harding, D.B. Satelle, and V.A. Bloomfield, editors. Royal Society of Chemistry Publishers, Cambridge, UK. 449 pp.
67. Lane, M.E., C.M. O'Driscoll, and O.I. Corrigan. 1996. The relationship between rat intestinal permeability and hydrophilic probe size. *Pharm. Res.* 13:1554–1558.
68. Solari, R., R.E. Offord, S. Remy, J.P. Aubry, T.N. Wells, E. Whitehorn, T. Oung, and A.E. Proudfoot. 1997. Receptor-mediated endocytosis of CC-chemokines. *J. Biol. Chem.* 272: 9617–9620.
69. Laurant, T.C., and J. Killander. 1964. A theory of gel filtration and its experimental verification. *J. Chromatogr.* 14:317–330.
70. Grotte, G. 1956. Passage of dextran molecules across the blood lymph barrier. *Acta Chir. Scand. Suppl. 2*11:1–84.
71. Cecil, R., and A.G. Ogston. 1949. Determination of sedimentation and diffusion constants of horse-radish peroxidase. *Biochem. J.* 49:105–112.
72. Kanwar, Y.S., and M.A. Venkatachalam. 1992. Ultrastructure

of glomerulus and juxtaglomerular apparatus. *In* Handbook of Physiology: Renal Physiology. Vol. I, Section 8. E.H. Windhager, editor. Oxford University Press, New York. 1–40.
73. Kent, S.P., and D.V. Wilson. 1975. Polysaccharides as labels for antibodies in electron microscopy. *J. Histochem. Cytochem.* 23:169–173.
74. Olszewski, W.L., and A. Engeset. 1978. Capillary transport of immunoglobulins and complement proteins to the interstitial fluid and lymph. *Arch. Immunol. Ther. Exp.* 26:57–65.
75. Meyer, F.A., M. Koblentz, and A. Silberberg. 1977. Structural investigation of loose connective tissue by using a series of dextran fractions as non-interacting macromolecular probes. *Biochem. J.* 161:285–291.